Results in Applied Mathematics 22 (2024) 100461

Contents lists available at ScienceDirect

Results in Applied Mathematics

journal homepage: www.elsevier.com/locate/results-in-applied-mathematics

# Uncovering a generalised gamma distribution: From shape to interpretation

Matthias Wagener [a,*], Andriette Bekker [a], Mohammad Arashi [b,a], Antonio Punzo [c]

[a] Department of Statistics, University of Pretoria, Lynnwood Street, Pretoria, 0002, Gauteng, South Africa
[b] Department of Statistics, Ferdowsi University of Mashhad, Azadi Square, Mashhad, 9177948974, Razavi Khorasan, Iran
[c] Department of Economics and Business, University of Catania, Corso Italia 55, Catania, 95129, Sicily, Italy

ARTICLE INFO

*Keywords:*
Body shape
Heavy-tails
Positive data
Insurance losses
Interpretability
Maximum likelihood estimation

ABSTRACT

In this paper, we introduce the flexible interpretable gamma (FIG) distribution, with origins in Weibulisation, power weighting, and a stochastic representation. The FIG parameters have been verified graphically, mathematically, and through simulation as having separable roles in influencing the left tail, body, and right tail shape. The generalised gamma (GG) distribution has become a standard model for positive data in statistics due to its interpretable parameters and tractable equations. Although there are many generalised forms of the GG that can provide a better fit to data, none of them extend the GG so that the parameters are interpretable. We conduct simulation studies on the maximum likelihood estimates and respective sub-models of the FIG. Finally, we assess the flexibility of the FIG relative to existing models by applying the FIG model to hand grip strength and insurance loss data.

## 1. Introduction

The best known form of the generalised gamma (GG) distribution was defined by Stacy and Hoshkin [1]. Before this, a precursor model had been analysed by Amoroso in 1925 for income distribution modelling purposes [2]. The GG contains numerous sub-models, including the exponential, gamma, Weibull, and log-normal, as limiting cases. The probability density function (PDF) of the standard (unscaled) GG is given below:

$$f(z;p,d)=\frac{p}{\Gamma(d/p)}z^{d-1}\mathrm{e}^{-z^p}, \tag{1}$$

where $z,d,p>0$, $\Gamma(\cdot)$ is the gamma function, and is denoted as $Z\sim GG(p,d)$. Note that (1) is equivalent to having $a=1$ in the PDF of Stacy and Hoshkin [1]. This is done as a simplification, with the knowledge that a simple scaling can be applied after generalisation. The role of the GG distribution shape parameters becomes apparent when considering the derivative of the log of the kernel in (1),

$$d(z;p,d)=\frac{\partial}{\partial z}\ln\left(z^{d-1}e^{-z^p}\right)=\frac{d-1}{z}-pz^{p-1}. \tag{2}$$

The left tail behaviour for GG is determined by $d$. Considering the case where, $d\neq 1$ and $\lim_{z\to 0^+}d(z;p,d)$ in (2), the first term dominates as the second approaches zero making $d$ the primary shape determinant. If $d=1$, it has no effect on the left tail shape. Fig. 1 illustrates these GG PDF properties in relation to $d$. The right tail behaviour for the GG is influenced by $p$. Considering the case where, $\lim_{z\to\infty}d(z;p,d)$ in (2), the first term approaches zero while the second dominates, thus making $p$ the primary shape

* Corresponding author.
*E-mail address:* matthias@dilectum.co.za (M. Wagener).

https://doi.org/10.1016/j.rinam.2024.100461
Received 22 January 2024; Received in revised form 7 April 2024; Accepted 30 April 2024
Available online 20 May 2024

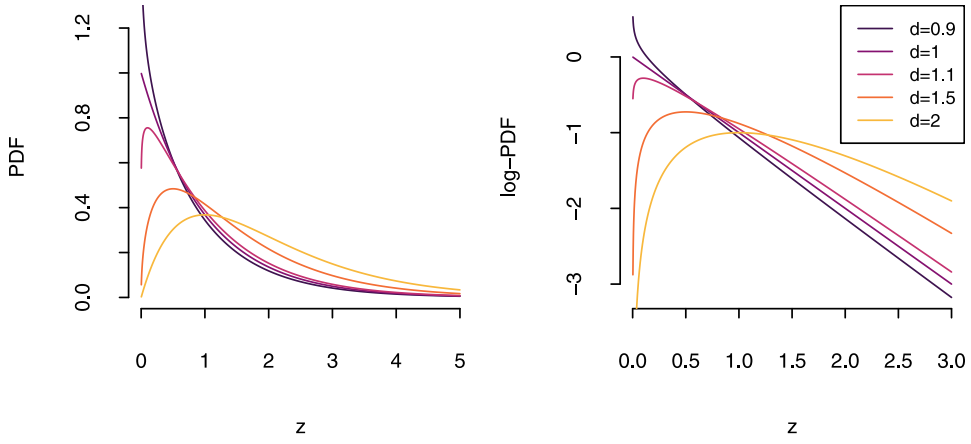


**Fig. 1.** The GG PDF for different values of left tail shape parameter $d$ and fixed right tail shape $p = 1$.

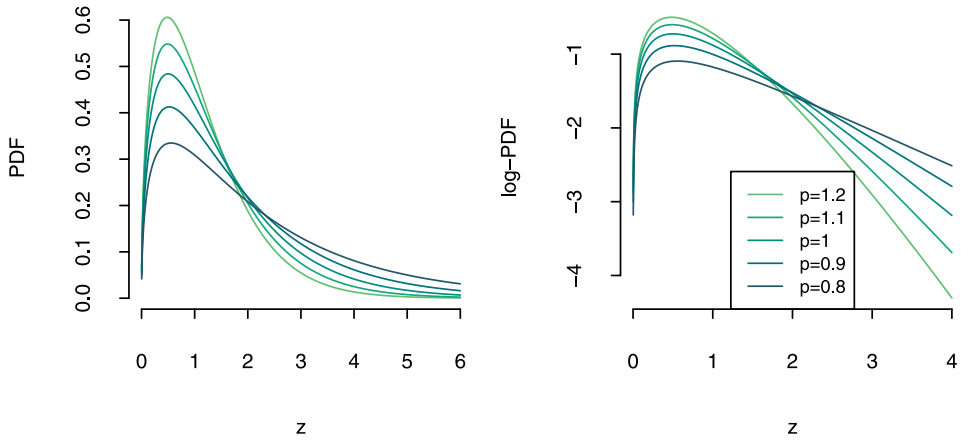


**Fig. 2.** The GG PDF for different values of the right tail shape parameter $p$ and fixed left tail shape $d = 1.5$.

determinant. Fig. 2 illustrates these GG PDF properties in relation to $p$. The broad range of distribution shapes for the GG can model has led to widespread application, such as in survival analysis [3], time series [4], phonemic segmentation [5], wireless fading models [6], drought [7], statistical size [8], demographic research [9], and economics [2]. Building on the success of the GG many authors have improved the applicability of the GG by the addition of parameters through generalisation. Generally speaking, the main excitement of these generalisations is their focus on superior fit in niche applications. In Table 1 a timeline of GG generalisations is given for completeness. The demands of new models today have a wider focus than simply better fit. The following authors, Ley [10], Jones [11], McLeish [12], Punzo and Bagnato [13], Wagener et al. [14], Ley et al. [15] specify these sometimes overlooked desirable qualities for new generalisations:

- A low number of interpretable parameters: These include parameters that control the distribution shape qualities such as or similar to location, scale, skewness, and kurtosis.
- Favourable estimation properties: It is important that the parameters can be estimated properly to ensure correct predictions and inferences from the model. Inferentially speaking, a generalised model for use in diagnosing distribution departure from a common baseline distribution.
- Simple mathematical tractability: Closed-form expressions and simple formulae aid in implementation, computational speed, and providing insight into the data.
- Finite moments: Most real-world measurements require this property.

Upon review of the literature in Table 1, only one of the generalisations, the $\kappa$-GG, has parameters that are easily interpreted. This is due to these parameters having overlapping influence in distribution shape, which then obfuscates their role in achieving a certain fit. The $\kappa$-GG is such a distribution because it has an extra right tail parameter which gives geometric instead of exponential tails. Another disadvantage of these distributions is that they lack simple formulas. This is due to the complex design of their generating mechanisms. The latter two points are viewed as an opportunity to develop a generalisation of the GG distribution.

**Table 1**
The timeline of the GG, its generalisations, and their number of parameters (including a scaling parameter).

| Distribution | Number of parameters | Author/s | Year |
|---|---|---|---|
| GG | 3 | Amoroso [2], Stacy and Hoshkin [1] | 1925,1962 |
| quotients of GG | 3 or $9ik$ for $i,k = 1,2,3,\ldots$ | Malik [16], Saieed et al. [17], Bilankulu et al. [18] | 1967,2020,2021 |
| log-GG | 3 | Consul and Jain [19], Prentice [20], Bell [21] | 1971,1974,1988 |
| unified GG | 4 | Agarwal and Kalla [22] | 1996 |
| composite Weibullised GG | 5 | Pauw et al. [23] | 2010 |
| exponentiated GG | 4 | Cordeiro et al. [24] | 2011 |
| Kumaraswamy GG | 5 | De Pascoa et al. [25] | 2011 |
| beta GG | 5 | Cordeiro et al. [26] | 2012 |
| Kummer beta GG | 6 | Cordeiro et al. [27] | 2014 |
| transmuted GG | 4 | Lucena et al. [28] | 2015 |
| weighted GG | 6 | Priyadarshani and Oluyede [29] | 2015 |
| $\kappa$−GG | 4 | Vallejos et al. [30], Kaniadakis [31] | 2018,2021 |
| Marshall–Olkin GG | 4 | Barriga et al. [32] | 2018 |
| double truncated GG | 5 | Bakery et al. [33] | 2021 |

Here, we systematically construct a generalisation of the GG distribution that possesses interpretable parameters, favourable estimation, simple formulae, and finite moments because of its generating mechanism and setup. This is done by power weighting the body-tail generalised normal distribution (BTN) [14] in order to have specific parameters for left tail shape, body shape, and right tail shape.

The paper is structured as follows. Section 2 illustrates the operations involved in generating positive real line distributions from symmetric distributions using Weibullisation and power weighting, and additionally, provides a stochastic representation of the flexible interpretable gamma distribution (FIG). Section 3 introduces the FIG, generated by the power weighting of the BTN baseline distribution; The section further presents derivations of the PDF, cumulative probability function (CDF), moments, moment generating function (MGF). Section 4 gives background information on maximum likelihood (ML) estimation. The roles of the FIG tail parameters are mathematically compared to the GG in Section 5. In Section 6 the parameters are proven to be identifiable. Section Section 7 evaluates the ML estimation of FIG sub-models, such as the flexible body exponential (FBE) and the flexible body gamma (FBG) sub-models, through simulation experiments. Section 8 applies the FIG to hand grip strength and insurance loss data. Section 9 summarises the results and key findings.

## 2. Origins of gamma-like distributions

In this section, we investigate three different situations that give rise to gamma-like distributions. This insight may then be used to guide an expansion of GG, with the aim of maintaining the shape and interpretable roles of the shape parameters.

*Weibullisation*

The Weibullisation for a given baseline distribution of a random variable $Z$ occurs when considering the random variable $Z^{1/\nu}$ for $\nu > 0$ [34]. If the baseline distribution is selected to be symmetrical, the Weibullisation of the random variable $|Z|$ yields a positive distribution which has a direct relationship to the shape of the baseline distribution. This process is illustrated for the GG distribution and its PDF in (1). As $|Z|$ is mathematically equivalent to one side or half of the baseline distribution due to symmetry, our analysis will continue with the latter. The GG distribution emerges when $Z$ follows a generalised normal (GN) distribution, see [35]. The PDF of the half-GN is given as:

$$f(z;s) = \frac{s}{\Gamma\left(\frac{1}{s}\right)} \mathrm{e}^{-z^s}, \tag{3}$$

where $z, s > 0$. Note that the half-GN contains the half-normal, half-Laplace, and uniform distributions for shape parameter values equal to $s = 2$, $s = 1$, and $s = \infty$, respectively [35]. Let $y = z^{1/\nu}$, then the PDF of the random variable $Y = Z^{1/\nu}$ is given by:

$$f(y;s,\nu) = \frac{s}{\Gamma\left(\frac{1}{s}\right)} y^{\nu-1} \mathrm{e}^{-y^{s\nu}}, \tag{4}$$

where $y, s > 0$. Comparing (1) and (4) shows that $Y$ follows a GG distribution with parameters $d = \nu$ and $p = s\nu$. In the kernel of (4), the right tail is determined by $\mathrm{e}^{-y^{s\nu}}$ and the left tail by $y^{\nu-1}$, refer to Section 1. A visual representation of this generating process of (4) is given in Fig. 3. Observe that $d$ affects the left tail shape, for $d = 1$ we have no change to the half baseline distribution, for $d < 1$ the left tail density is increased, and for $d > 1$ the left tail density is decreased. The left tail shape does not influence the right tail, apart from a change of overall scale in the Weibullised distribution. The behaviour of the right tail is left to be determined by the half baseline distribution kernel from (3) in this instance.

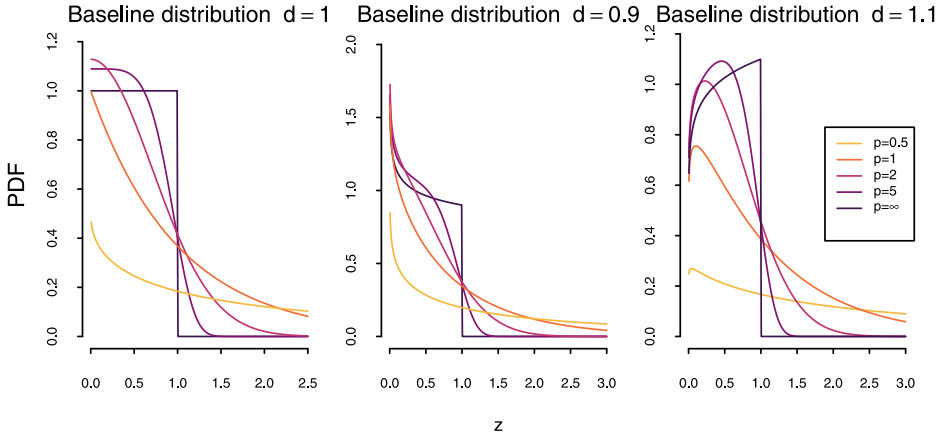


**Fig. 3.** Examples of different Weibullisations of the half-GN equivalent to GG with different left tail shapes $d$ and body shapes $p$.

*Power weighted distributions*

The GG distribution (1) also arises in the power weighted kernel of the integrand of the $r$th absolute moments of the GN distribution. In general, if the absolute $r$th moments of a distribution $Z$ exist and are finite, a positive distribution $Y$ can be generated from it. Consider the absolute $r$th moment of $Z$:

$$E(|Z|^r) = \int_{\mathbb{R}} |z|^r f(z) dz, \tag{5}$$

where $r > 0$. The integrand is a valid kernel for a positive support distribution since its integral is finite by definition. Therefore, a new PDF can be generated by normalising the integrand function with the actual value of the integral, with the new PDF given by:

$$f(y; r) = \frac{y^r f(y)}{E(|Z|^r)}, \tag{6}$$

where $y, r > 0$ and $f(\cdot)$ is the original PDF of $Z$. To generate the GG PDF in this manner, $Z$ is taken as the GN distribution. By substituting (3) into (6) the generated PDF of $Y$ is given by:

$$f(y; r, s) = \frac{s}{\Gamma\left(\frac{r}{s}\right)} y^r \mathrm{e}^{-y^s}, \tag{7}$$

where $y, r, s > 0$. Subsequently, from (7), we have that $Y$ follows a GG distribution with $d = r + 1$ and $p = s$.

*Scale mixture model*

The FIG distribution also arises through a scale mixture of power-function (PF) distributions, which is a special case of the beta distribution [36]. Even if this kind of mixture cannot represent the GG, we still include it in this section, since it gives rise to the FIG distribution, which has gamma-like properties. The PDF of the scaled PF distribution is given below:

$$f(x; u, \nu) = \frac{\nu}{u^\nu} x^{\nu-1}, \tag{8}$$

where $0 < x \leq u, u > 0, \nu > 0$, and is denoted as $X \sim PF(u, \nu)$.

**Theorem.** *Let $Z \sim PF(u, \nu)$ and $u \sim GG(\beta, \alpha)$, then the PDF of $Z$ is given by:*

$$f(z; \alpha, \beta, \nu) = \frac{\nu z^{\nu-1}}{\Gamma\left(\frac{\alpha+\nu}{\beta}\right)} \Gamma\left(\frac{\alpha}{\beta}, z^\beta\right). \tag{9}$$

**Proof.** Using the pre-defined random variables $Z$ and $U$, noting that $Z < U$ by definition, and employing the indicator variable $I(\cdot)$ we have the following:

$$f(z; \alpha, \beta, \nu) = \int_{\mathbb{R}} I(z \leq u) \frac{\nu}{u^\nu} z^{\nu-1} \frac{u^{\alpha+\nu-1} e^{-u^\beta}}{\Gamma\left(\frac{\alpha+\nu}{\beta}\right)} du \tag{10}$$

$$= \frac{\nu z^{\nu-1}}{\Gamma\left(\frac{\alpha+\nu}{\beta}\right)} \int_z u^{\alpha-1} e^{-u^\beta} du \tag{11}$$

$$= \frac{\nu z^{\nu-1}}{\Gamma\left(\frac{\alpha+\nu}{\beta}\right)} \Gamma\left(\frac{\alpha}{\beta}, z^{\beta}\right), \tag{12}$$

which concludes the proof.

*Conclusion*

In the selection of a baseline distribution, it is important to consider the existing roles of shape parameters and symmetry. This is crucial since any ambiguous roles pertaining to the baseline distribution parameters will inevitably be transferred to the distributions that are subsequently generated. Hence, it is not recommended to use asymmetric distributions due to the uncertainty of the effects of the asymmetry parameter following generalisation. This section presented three different methods of obtaining GG type distributions. To derive the FIG distribution, our preference lies with the power weighted and scale mixture origins' parameterisations, details of which will be extensively discussed in the subsequent section.

## 3. The flexible interpretable gamma distribution

This section consists of the motivation for the chosen FIG baseline distribution and the derivations of the PDF, CDF, moments, and MGF for the standard and scaled FIG distribution.

*Baseline distribution*

The baseline distribution for the FIG is the BTN distribution. The BTN distribution is a generalisation of the GN and normal distribution which has interpretable parameters, simple mathematical tractability, and finite moments. The latter desirable properties will be transferred to the FIG distribution in the same way the power weighting of the GN transferred its properties to the GG. The PDF of the BTN is:

$$f(z;\alpha,\beta) = \frac{\Gamma\left(\frac{\alpha}{\beta}, |z|^{\beta}\right)}{2\Gamma\left(\frac{\alpha+1}{\beta}\right)}, \tag{13}$$

where $z \in \mathbb{R}, \alpha, \beta > 0$, and $\Gamma(\cdot,\cdot)$ is the upper incomplete gamma function [37, p. 899]. The parameters have clear roles, where $\alpha$ determines body shape and $\beta$ determines the tail shape of the distribution. Note that, for $\alpha = \beta = s$, (13) is equivalent to (3), making the GN and its nested models a subset of the BTN; for more details refer to [14]. Due to the latter fact, the power weighting of the BTN will therefore contain the GG distribution for $\alpha = \beta$ as discussed in Section 2. The absolute moments of the BTN are given by:

$$E(|Z|^{r}) = \frac{\Gamma\left(\frac{\alpha+r+1}{\beta}\right)}{(r+1)\Gamma\left(\frac{\alpha+1}{\beta}\right)}, \tag{14}$$

where $r > 0$; see [14]. In Fig. 4 the different body shapes for a fixed tail shape can be seen. Similarly, in Fig. 5 the different tail shapes for a given body shape is shown. The additional body shape parameter of the BTN specifically enhances the body shape of the GG distribution through power weighting in the FIG distribution. Therefore, the additional $\alpha$ parameter has an interpretation and provides information about the body shape of the FIG. Fig. 6 illustrates this process of power weighting and the effect of the body shape parameter $\alpha$. Here, the GG and its fixed body shape is shown for $\alpha = \beta = 2$. Notice that in the region of the body, $0.5 < z < 1$, the shape is determined by $\alpha$. In the region of the left tail, $z < 0.5$, the shape is determined by $\nu$. In the region of the right tail, $z > 1$, the shape is determined by $\beta$. Importantly, note that both the tail shapes stay markedly the same for different body shapes $\alpha$.

The FIG has extended the GG body shapes to "steeper" and "flatter" for body shapes where $\alpha \neq \beta$, while endeavouring to maintain the roles of the left and right tail parameters, $\nu$ and $\beta$, as closely as possible. Changes in body shape do marginally affect the tail shapes since altering the body shape redistributes probability density across different regions of the domain. The rationale behind the separability of the parameters and their functions is validated through visual confirmation as described above, quantifying the difference of the derivatives of the log-PDF in the left and right tails of the distribution (Section 5). Then ensuring the FIG model is mathematically identifiable (Section 6). Additionally, simulating sub-models of the FIG offers insight into the separability of the body shape from the left and right tail parameters in the data, while also determining the sample size required for accurately identifying the body shape (Section 7).

In summary, the FIG distribution derives its unique properties from the BTN. The main property of interest is that each shape parameter controls either the left tail, body, or right tail behaviour of the FIG. The FIG provides for greater flexibility in conjunction with numerically interpretable values for the cause of deviation from the GG.

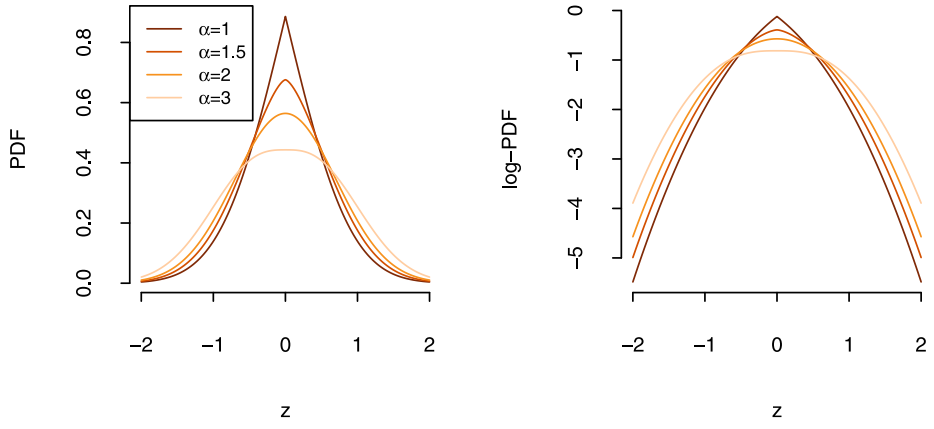


**Fig. 4.** Examples of BTN PDFs for different values of body shape $\alpha$ and fixed tail shape $\beta = 2$.

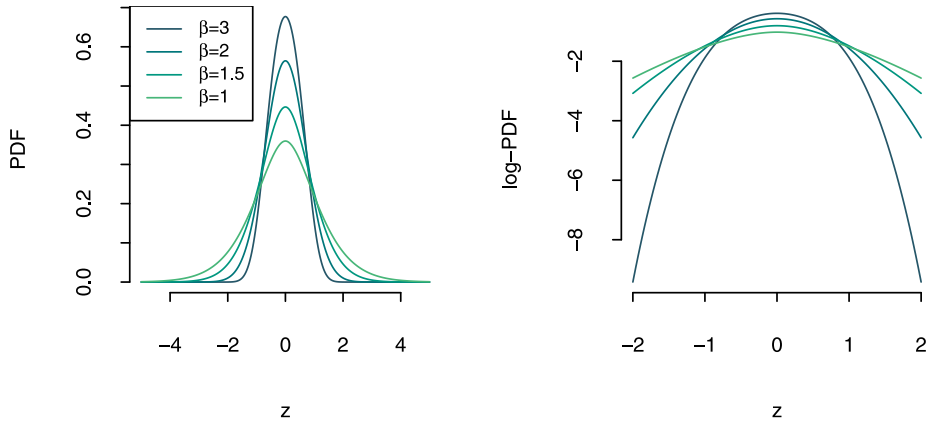


**Fig. 5.** The BTN PDF for different values of tail shape $\beta$ and fixed body shape $\alpha = 2$.

*PDF*

The FIG PDF is derived by substituting (13) and (14) into (6) and is given below:

$$f(z;\alpha,\beta,\nu) = \frac{\nu z^{\nu-1}}{\Gamma\left(\frac{\alpha+\nu}{\beta}\right)}\Gamma\left(\frac{\alpha}{\beta}, z^{\beta}\right), \tag{15}$$

where $z, \alpha, \beta, \nu > 0$ denoted as $Z \sim FIG(\alpha, \beta, \nu)$. We note that if $\alpha = \beta$, then we have the standard GG distribution with parameters $p = \nu$ and $d = \alpha$. A depiction of the FIG PDF (15) and corresponding baseline PDF is given in Fig. 6. The PDF of the scaled FIG, denoted as $X \sim FIG(\sigma, \alpha, \beta, \nu)$, is obtained using the transformation $X = \sigma Z$:

$$f(x;\sigma,\alpha,\beta,\nu) = \frac{\nu x^{\nu-1}}{\sigma^{\nu}\Gamma\left(\frac{\alpha+\nu}{\beta}\right)}\Gamma\left(\frac{\alpha}{\beta}, \left(\frac{x}{\sigma}\right)^{\beta}\right), \tag{16}$$

where $\sigma > 0$.

*CDF*

The CDF of the standard FIG is derived with the definition of a CDF and (15):

$$F(z;\alpha,\beta,\nu) = \int_{-\infty}^{z} \frac{\nu t^{\nu-1}}{\Gamma\left(\frac{\alpha+\nu}{\beta}\right)}\Gamma\left(\frac{\alpha}{\beta}, t^{\beta}\right) dt$$

$$= \frac{\nu}{\Gamma\left(\frac{\alpha+\nu}{\beta}\right)}\left[\int_{0}^{\infty} t^{\nu-1}\Gamma\left(\frac{\alpha}{\beta}, t^{\beta}\right) dt - \int_{z}^{\infty} t^{\nu-1}\Gamma\left(\frac{\alpha}{\beta}, t^{\beta}\right) dt\right].$$

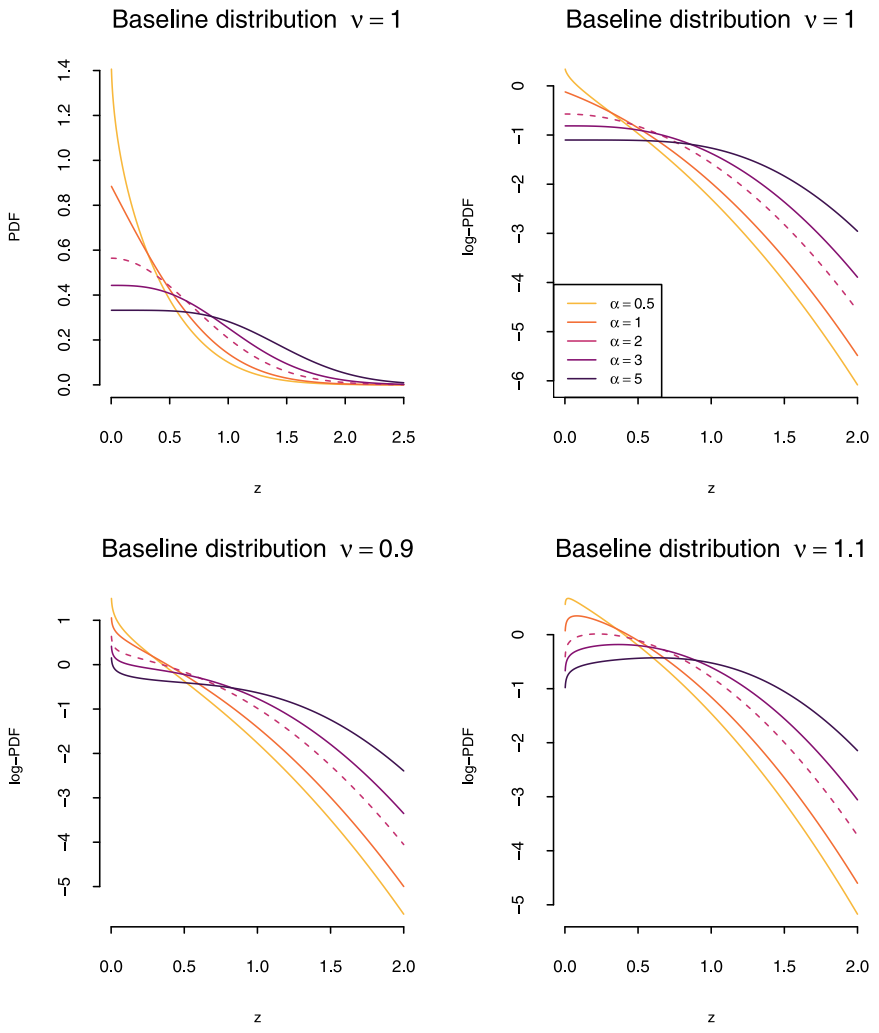


**Fig. 6.** The baseline BTN and generated FIG PDFs for different body and left tail shape parameters with fixed right tail shape ($\beta = 2$) are shown in the first row (half baseline distributions) and second row (corresponding generated distributions).

Applying Lemma 2 of the Appendix to both integrals, we have that:

$$F(z;\alpha,\beta,\nu) = \frac{\nu}{\Gamma\left(\frac{\alpha+\nu}{\beta}\right)}\left[\lim_{t\to 0^+}\frac{\Gamma\left(\frac{\alpha+\nu}{\beta},t^\beta\right)t^\nu\Gamma\left(\frac{\alpha}{\beta},t^\beta\right)}{\nu} - \frac{\Gamma\left(\frac{\alpha+\nu}{\beta},z^\beta\right) - z^\nu\Gamma\left(\frac{\alpha}{\beta},z^\beta\right)}{\nu}\right]$$
$$= \frac{\gamma\left(\frac{\alpha+\nu}{\beta},z^\beta\right) + z^\nu\Gamma\left(\frac{\alpha}{\beta},z^\beta\right)}{\Gamma\left(\frac{\alpha+\nu}{\beta}\right)}, \tag{17}$$

where $\gamma(\cdot,\cdot)$ is the lower incomplete gamma function [37, p.899]. Subsequently, the CDF of $X \sim FIG(\sigma,\alpha,\beta,\nu)$ is given by the substitution of $z = \frac{x}{\sigma}$ in (17).

*FIG sub-models*

The scaled FIG distribution, an extension of the FIG, incorporates various sub-models detailed in Table 2. These sub-models offer practical utility in applications requiring specific distributions either based on prior knowledge or for model simplicity. Notable examples of such sub-models include exponential, gamma, half-normal, and Weibull distributions. In these sub-models, if $\alpha \neq \beta$ the body shape is enhanced, enabling the FIG distribution to effectively model diverse datasets while maintaining simplicity.

The relevant statistical properties for the sub-models in Table 2 can be obtained by substituting the relevant parameters into the FIG distribution equations. In Section 7, the focus will be on two specific sub-models, namely the flexible body exponential (FBE);

**Table 2**
A summary of nested models of the FIG distribution.

| Distribution | $\sigma$ | $\alpha$ | $\beta$ | $\nu$ |
|---|---|---|---|---|
| Chi-squared | 2 | 1 | 1 | $df/2$ |
| Exponential | $1/\lambda$ | 1 | 1 | 1 |
| Gamma | $\theta$ | 1 | 1 | $k$ |
| GG | $a$ | $p$ | $p$ | $d$ |
| Half-BTN | $\sigma$ | $\alpha$ | $\beta$ | 1 |
| Half-PN | $\sigma$ | $s$ | $s$ | 1 |
| Half-normal | $\sqrt{2}\sigma$ | 2 | 2 | 1 |
| Maxwell–Boltzmann | $\sqrt{2}a$ | 2 | 2 | 3 |
| Rayleigh | $\sqrt{2}\sigma$ | 2 | 2 | 2 |
| Uniform | 1 | $\infty$ | $\infty$ | 1 |
| Weibull | $\lambda$ | $k$ | $k$ | $k$ |

($X \sim FBE(\sigma,\alpha)$) and the flexible body gamma (FBG); ($X \sim FBG(\sigma,\alpha,\nu)$), notable for their emphasis on altering the body shape rather than the left or right tails.

*Mode*

The maximum of the standard FIG PDF is given by the maximum of the FIG kernel in (15). We consider two cases for obtaining the mode of the FIG. For $\nu \leq 1$ we have that

$$\lim_{z\to 0^+} z^{\nu-1}\Gamma\left(\frac{\alpha}{\beta}, z^\beta\right) = \infty, \tag{18}$$

and

$$\lim_{z\to \infty} z^{\nu-1}\Gamma\left(\frac{\alpha}{\beta}, z^\beta\right) = 0, \tag{19}$$

which implies that the mode is zero. For $\nu > 1$ we have that

$$\begin{aligned}\frac{\partial}{\partial z} z^{\nu-1}\Gamma\left(\frac{\alpha}{\beta}, z^\beta\right) &= (\nu-1)(z^{\nu-2})\Gamma\left(\frac{\alpha}{\beta}, z^\beta\right) + z^{\nu-1}\left(-z^{\beta(\frac{\alpha}{\beta}-1)}e^{-z^\beta}\beta z^{\beta-1}\right)\\ &= (\nu-1)(z^{\nu-2})\Gamma\left(\frac{\alpha}{\beta}, z^\beta\right) - z^{\nu-2}\left(z^\alpha e^{-z^\beta}\beta\right)\\ &= z^{\nu-2}\left[(\nu-1)\Gamma\left(\frac{\alpha}{\beta}, z^\beta\right) - \beta z^\alpha e^{-z^\beta}\right].\end{aligned} \tag{20}$$

Examining the elements inside the brackets in (20), we find that for

$$\lim_{z\to 0^+}(\nu-1)\Gamma\left(\frac{\alpha}{\beta}, z^\beta\right) = (\nu-1)\Gamma\left(\frac{\alpha}{\beta}\right) > \lim_{z\to 0^+}\beta z^\alpha e^{-z^\beta} = 0, \tag{21}$$

which implies (20) is greater than zero for some $z$. Since both terms in (20) are greater than zero for all $z$, we investigate the rate of decrease for these functions as $z$ increases. The relative rate of decrease for the left and right terms in (20) with respect to $z$ is given by

$$\frac{\frac{\partial}{\partial z}\beta z^\alpha e^{-z^\beta}}{\frac{\partial}{\partial z}(\nu-1)\Gamma\left(\frac{\alpha}{\beta}, z^\beta\right)} = \frac{\beta\left[\alpha z^{\alpha-1}e^{-z^\beta} + z^\alpha e^{-z^\beta}\left(-\beta z^{\beta-1}\right)\right]}{(\nu-1)\left(-\beta z^{\alpha-1}e^{-z^\beta}\right)} = \frac{\beta z^\beta - \alpha}{\nu-1}, \tag{22}$$

which implies that $\beta z^\alpha e^{-z^\beta}$ decreases geometrically faster than $(\nu-1)\Gamma\left(\frac{\alpha}{\beta}, z^\beta\right)$ for $z > \frac{\ln(\alpha)-\ln(\beta)}{\beta}$. Noting that $(\nu-1)\Gamma\left(\frac{\alpha}{\beta}, z^\beta\right)$ is monotonically decreasing, and $\beta z^\alpha e^{-z^\beta}$ is increasing and then decreasing but at a slower relative rate for all $z$ we have that (20) is negative from some $z$ onward. Therefore, we have that PDF of the is first increasing and then decreasing for $\nu > 1$ implying a mode which can be numerically calculated by setting (20) to zero.

*Moments*

The $r$th moment of the standard FIG is derived from (15), and Lemma 3 in the Appendix:

$$E(Z^r) = \frac{\nu\Gamma\left(\frac{\alpha+\nu+r}{\beta}\right)}{(\nu+r)\Gamma\left(\frac{\alpha+\nu}{\beta}\right)}. \tag{23}$$

Subsequently, the $r$th moment of $X \sim FIG(\sigma,\alpha,\beta,\nu)$ is given by (23), and the identity $E(X^r) = \sigma^r E(Z^r)$.

*Moment generating function*

From the definition of a MGF, (15) and the series expansion of the incomplete gamma function [37, p. 901]. The MGF of the standard FIG is derived by:

$$M_z(t) = \frac{\nu}{\Gamma\left(\frac{\alpha+\nu}{\beta}\right)} \sum_{n=0}^{\infty} \frac{t^n \Gamma\left(\frac{\nu+n+\alpha}{\beta}\right)}{n!(\nu+n)}. \tag{24}$$

Subsequently, the MGF of $X \sim BTN(\mu, \sigma, \alpha, \beta)$ is given by (24), and the identity $M_X(t) = \mathrm{e}^{t\mu} M_Z(t\sigma)$.

## 4. FIG maximum likelihood equations

The log-likelihood (LL) for a random sample $x_1, x_2, \ldots, x_n$ from $X \sim FIG(\sigma, \alpha, \beta, \nu)$ observations is

$$\begin{aligned} \mathrm{LL}(\sigma, \alpha, \beta, \nu; x_1, x_2, \ldots, x_n) = \sum_{i=1}^{n} \Bigg[ & \ln(\nu) - \ln(\sigma) + (\nu - 1)\ln(z_i) \\ & + \ln\left(\Gamma\left(\frac{\alpha}{\beta}, z_i^{\beta}\right)\right) - \ln\left(\Gamma\left(\frac{\alpha+\nu}{\beta}\right)\right)\Bigg], \end{aligned} \tag{25}$$

where $z_i = x_i/\sigma$. The derivatives of the individual terms in (25) with respect to the FIG parameters are given by:

$$\begin{aligned} \frac{\partial LL}{\partial \sigma} &= -\frac{\nu}{\sigma} - \frac{\beta z_i^{\beta} \Psi_2\left(\frac{\alpha}{\beta}, z_i^{\beta}\right)}{\sigma \Gamma\left(\frac{\alpha}{\beta}, z_i^{\beta}\right)} \\ \frac{\partial LL}{\partial \alpha} &= \frac{\Psi_1\left(\frac{\alpha}{\beta}, z_i^{\beta}\right)}{\beta \Gamma\left(\frac{\alpha}{\beta}, z_i^{\beta}\right)} - \frac{\psi\left(\frac{\alpha+\nu}{\beta}\right)}{\beta} \\ \frac{\partial LL}{\partial \beta} &= \frac{\Psi_3\left(\frac{\alpha}{\beta}, z_i^{\beta}, \beta\right)}{\Gamma\left(\frac{\alpha}{\beta}, z_i^{\beta}\right)} + \frac{\psi\left(\frac{\alpha+\nu}{\beta}\right)(\alpha+\nu)}{\beta^2} \\ \frac{\partial LL}{\partial \nu} &= \frac{1}{\nu} + \ln(z_i) - \frac{\psi\left(\frac{\alpha+\nu}{\beta}\right)}{\beta}, \end{aligned}$$

where

$$\begin{aligned} \Psi_1(u, v) &= \frac{\partial}{\partial u}\Gamma(u, v) = \Gamma(u, v)\ln v + A(u, v), \\ \Psi_2(u, v) &= \frac{\partial}{\partial v}\Gamma(u, v) = -v^{u-1}\mathrm{e}^{-v}, \\ \Psi_3(u, v, w) &= \Psi_1(u, v)\frac{\partial}{\partial w}u + \Psi_2(u, v)\frac{\partial}{\partial w}v, \\ A(u, v) &= G_{2,3}^{3,0}\left(v \,\middle|\, \begin{matrix} 1, 1 \\ 0, 0, u \end{matrix}\right), \end{aligned}$$

$\psi(\cdot)$ is the digamma function, and $G$ is the Meijer's G function [37, p.850,902].

## 5. FIG tail parameter behaviour

To examine the behaviour of the left and right tail of the FIG in comparison to the GG, we examine the derivative of the difference of log-kernel functions between the FIG and GG as follows:

$$\begin{aligned} d(z; \alpha, \beta, \nu) &= \frac{\partial}{\partial z}\left[\ln\left(z^{\nu-1}\Gamma\left(\frac{\alpha}{\beta}, z^{\beta}\right)\right) - \ln\left(z^{\nu-1}e^{-z^{\beta}}\right)\right] \\ &= \frac{\partial}{\partial z}\left[\ln\left(\Gamma\left(\frac{\alpha}{\beta}, z^{\beta}\right)\right) - z^{\beta}\right] \\ &= \frac{-\left(z^{\beta}\right)^{\frac{\alpha}{\beta}-1} e^{-z^{\beta}}\left(-\beta z^{\beta-1}\right)}{\Gamma\left(\frac{\alpha}{\beta}, z^{\beta}\right)} - \beta z^{\beta-1} \\ &= \frac{-\beta z^{\alpha-1} e^{-z^{\beta}}}{\Gamma\left(\frac{\alpha}{\beta}, z^{\beta}\right)} - \beta z^{\beta-1}. \end{aligned} \tag{26}$$

Comparing the left tail behaviour of the FIG to the GG, we evaluate

$$\lim_{z\to 0^+} d(z;\alpha,\beta,\nu) = 0\times 1 - 0 = 0, \tag{27}$$

which suggests that the left tail behaviour of the FIG approximates the shape of the GG distribution for small $z$. This property is visually confirmed by the bottom left sub-figure of Fig. 6. Regarding, the right tail behaviour, we first concentrate on the first term in (26) for large values of $z$. The limit is of the form zero divided by zero, for which we apply L'Hôpital's rule:

$$\begin{aligned}
&\lim_{z\to\infty} \frac{-\beta z^{\alpha-1}e^{-z^\beta}}{\Gamma\left(\frac{\alpha}{\beta}, z^\beta\right)} \\
&\overset{L'H}{=} \lim_{z\to\infty} \frac{-\beta\left[(\alpha-1)(z^{\alpha-z}e^{-z^\beta}) + (z^{\alpha-1}e^{-z^\beta})\left(-\beta z^{\beta-1}\right)\right]}{-\beta z^{\alpha-1}e^{-z^\beta}} \\
&= \lim_{z\to\infty} (\alpha-1)z^{-1} - z^{\beta-1} \\
&= -z^{\beta-1}.
\end{aligned} \tag{28}$$

Substituting the result from (28) into $\lim_{z\to\infty} d(z;\alpha,\beta,\nu) = 0$, we conclude that the FIG right tail behaviour approximates the shape of the GG distribution for large $z$. Similarly, this property is visually confirmed by the bottom right sub-figure of Fig. 6. It is worth noting that the body shape parameter $\alpha$ does not influence calculated left and right tail limits, suggesting that the left and right tail parameters have maintained their roles and interpretation.

## 6. FIG identifiability

The FIG distribution is derived with the intent of gaining insights from the fitted parameters to data. It is, therefore, important that the parameters of the FIG PDF (16) are mathematically identifiable.

**Theorem.** *Let $X \sim FIG(\sigma,\alpha,\beta,\nu)$. If $\sigma_1,\sigma_2>0, \alpha_1,\alpha_2>0, \beta_1,\beta_2>0, \nu_1,\nu_2>0$ such that $f\left(x;\sigma_1,\alpha_1,\beta_1,\nu_1\right) = f\left(x;\sigma_2,\alpha_2,\beta_2,\nu_2\right), \forall x>0$ then $\sigma_1=\sigma_2, \alpha_1=\alpha_2, \beta_1=\beta_2, \nu_1=\nu_2$.*

**Proof.** The proof follows by the method of contradiction, assume the parameters of the FIG are not identifiable. That is, there exist parameters $\sigma_1\neq\sigma_2, \alpha_1\neq\alpha_2, \beta_1\neq\beta_2, \nu_1\neq\nu_2$ such that

$$f\left(x;\sigma_1,\alpha_1,\beta_1,\nu_1\right) = f\left(x;\sigma_2,\alpha_2,\beta_2,\nu_2\right), \tag{29}$$

where $\sigma_1,\sigma_2,\alpha_1,\alpha_2,\beta_1,\beta_2,\nu_1,\nu_2>0$. From the hypothesis (29) and substitution of (16) we have that

$$\frac{\nu_1 x^{\nu_1-1}\Gamma\left(\frac{\alpha_1}{\beta_1}, \left(\frac{x}{\sigma_1}\right)^{\beta_1}\right)}{\sigma_1^{\nu_1}\Gamma\left(\frac{\alpha_1+\nu_1}{\beta_1}\right)} = \frac{\nu_2 x^{\nu_2-1}\Gamma\left(\frac{\alpha_2}{\beta_2}, \left(\frac{x}{\sigma_2}\right)^{\beta_2}\right)}{\sigma_2^{\nu_2}\Gamma\left(\frac{\alpha_2+\nu_2}{\beta_2}\right)}, \forall x>0,$$

from which we obtain

$$\frac{x^{\nu_1-\nu_2}\Gamma\left(\frac{\alpha_1}{\beta_1}, \left(\frac{x}{\sigma_1}\right)^{\beta_1}\right)}{\Gamma\left(\frac{\alpha_2}{\beta_2}, \left(\frac{x}{\sigma_2}\right)^{\beta_2}\right)} = \frac{\nu_2\sigma_1^{\nu_1}\Gamma\left(\frac{\alpha_1+\nu_1}{\beta_1}\right)}{\nu_1\sigma_2\nu_2\Gamma\left(\frac{\alpha_2+\nu_2}{\beta_2}\right)}, \forall x>0. \tag{30}$$

Assuming for contradiction that $\nu_1\neq\nu_2$. It would now be possible that

$$\lim_{x\to 0^+} \frac{x^{\nu_1-\nu_2}\Gamma\left(\frac{\alpha_1}{\beta_1}, \left(\frac{x}{\sigma_1}\right)^{\beta_1}\right)}{\Gamma\left(\frac{\alpha_2}{\beta_2}, \left(\frac{x}{\sigma_2}\right)^{\beta_2}\right)} = \begin{cases} 0^+ & \text{se} \quad \nu_1>\nu_2 \\ +\infty & \text{se} \quad \nu_1<\nu_2, \end{cases}$$

which is in contradiction with the equality in (29) where $\frac{\nu_2\sigma_1^{\nu_1}\Gamma\left(\frac{\alpha_1+\nu_1}{\beta_1}\right)}{\nu_1\sigma_2\nu_2\Gamma\left(\frac{\alpha_2+\nu_2}{\beta_2}\right)} \in \mathbb{R}^+$. Therefore, it must necessarily be that $\nu_1=\nu_2$. We therefore substitute $\nu=\nu_1=\nu_2$ from here on forward. From (29), it follows that:

$$\begin{aligned}
&\Gamma\left(\frac{\alpha_1}{\beta_1}, \left(\frac{x}{\sigma_1}\right)^{\beta_1}\right) = \frac{\sigma_1^{\nu}\Gamma\left(\frac{\alpha_1+\nu}{\beta_1}\right)}{\sigma_2^{\nu}\Gamma\left(\frac{\alpha_2+\nu}{\beta_2}\right)}\Gamma\left(\frac{\alpha_2}{\beta_2}, \left(\frac{x}{\sigma_2}\right)^{\beta_2}\right), \forall x>0, \\
&\Gamma\left(\frac{\alpha_1}{\beta_1}, \left(\frac{x}{\sigma_1}\right)^{\beta_1}\right) = k\Gamma\left(\frac{\alpha_2}{\beta_2}, \left(\frac{x}{\sigma_2}\right)^{\beta_2}\right), \forall x>0,
\end{aligned} \tag{31}$$

where $k = \frac{\sigma_1^{\nu}\Gamma\left(\frac{\alpha_1+\nu}{\beta_1}\right)}{\sigma_2^{\nu}\Gamma\left(\frac{\alpha_2+\nu}{\beta_2}\right)} > 0$. Taking the derivative of both sides of (31) with respect to $x$, we obtain

$$-\left(\frac{x}{\sigma_1}\right)^{\beta_1\left(\frac{\alpha_1}{\beta_1}-1\right)} e^{-\left(\frac{x}{\sigma_1}\right)^{\beta_1}} \frac{\beta_1}{\sigma_1}\left(\frac{x}{\sigma_1}\right)^{\beta_1-1} = -k\left(\frac{x}{\sigma_2}\right)^{\beta_2\left(\frac{\alpha_2}{\beta_2}-1\right)} e^{-\left(\frac{x}{\sigma_2}\right)^{\beta_2}} \frac{\beta_2}{\sigma_2}\left(\frac{x}{\sigma_2}\right)^{\beta_2-1}, \forall x > 0.$$

After rearranging, it follows that

$$x^{\alpha_1-\alpha_2} e^{\left(\frac{x}{\sigma_2}\right)^{\beta_2}-\left(\frac{x}{\sigma_1}\right)^{\beta_1}} = \frac{k\beta_2\sigma_1^{\alpha_1}}{\beta_1\sigma_2^{\alpha_2}}, \forall x > 0. \tag{32}$$

Assuming for contradiction that $\alpha_1 \neq \alpha_2$. It would now be possible that

$$\lim_{x\to 0^+} x^{\alpha_1-\alpha_2} e^{\left(\frac{x}{\sigma_2}\right)^{\beta_2}-\left(\frac{x}{\sigma_1}\right)^{\beta_1}} = \begin{cases} 0^+ & \text{if} \quad \alpha_1 > \alpha_2 \\ +\infty & \text{if} \quad \alpha_1 < \alpha_2, \end{cases}$$

which is in contradiction with the equality in (32), since $\frac{k\beta_2\sigma_1^{\alpha_1}}{\beta_1\sigma_2\alpha_2} \in \mathbb{R}^+$. Therefore, it must necessarily be that $\alpha_1 = \alpha_2$. We therefore substitute $\alpha = \alpha_1 = \alpha_2$. Consequently, (32) simplifies to:

$$e^{\left(\frac{x}{\sigma_2}\right)^{\beta_2}-\left(\frac{x}{\sigma_1}\right)^{\beta_1}} = \frac{k\beta_2\sigma_1^{\alpha}}{\beta_1\sigma_2^{\alpha}}, \forall x > 0. \tag{33}$$

Assuming for contradiction that $\beta_1 \neq \beta_2$. It would now be possible that

$$\lim_{x\to+\infty} e^{\left(\frac{x}{\sigma_2}\right)^{\beta_2}-\left(\frac{x}{\sigma_1}\right)^{\beta_1}} = \begin{cases} 0^+ & \text{if} \quad \beta_1 > \beta_2 \\ +\infty & \text{if} \quad \beta_1 < \beta_2, \end{cases}$$

which is in contradiction with the equality in (33), since $\frac{k\beta_2{\sigma_1}^{\alpha}}{\beta_1{\sigma_2}^{\alpha}} \in \mathbb{R}^+$. Therefore, it must necessarily be that $\beta_1 = \beta_2$. We therefore substitute $\beta = \beta_1 = \beta_2$ from here on forward. Consequently, (33) simplifies to:

$$e^{\left(\frac{x}{\sigma_2}\right)^{\beta}-\left(\frac{x}{\sigma_1}\right)^{\beta}} = \frac{k\sigma_1^{\alpha}}{\sigma_2^{\alpha}}, \forall x > 0. \tag{34}$$

Assuming for contradiction that $\sigma_1 \neq \sigma_2$. It would now be possible that

$$\lim_{x\to+\infty} e^{\left(\frac{x}{\sigma_2}\right)^{\beta}-\left(\frac{x}{\sigma_1}\right)^{\beta}} = \lim_{x\to+\infty} e^{\frac{\sigma_1^{\beta}-\sigma_2\beta}{\sigma_2\beta\sigma_1\beta}x^{\beta}} = \begin{cases} +\infty & \text{if} \quad \sigma_1 > \sigma_2 \\ 0^+ & \text{if} \quad \sigma_1 < \sigma_2, \end{cases}$$

which is in contradiction with the equality in (34), since $\frac{k\sigma_1^{\alpha}}{\sigma_2^{\alpha}} \in \mathbb{R}^+$. Therefore, it must necessarily be that $\sigma_1 = \sigma_2$. In summary, it has been proven that $\sigma_1 = \sigma_2, \alpha_1 = \alpha_2, \beta_1 = \beta_2, \nu_1 = \nu_2$ which completes the proof.

## 7. Simulation study

In this section, we explore the properties of ML estimates for the FBE and FBG distributions, which are flexible versions derived from the exponential and gamma distributions. Metrics including bias and root mean squared error (RMSE) are calculated for samples generated using the stochastic representation (9). The numerical estimation starting parameters will be the ML of the exponential distribution, as the exponential distribution is a sub-model of FBE and FBG. The simulation is implemented using the NumPy [38] and SciPy [39] libraries in Python.

The simulation focuses on $X \sim FBE(10, 4)$ and $X \sim FBG(10, 4, 0.9)$, highlighting how the FBE and FBG distributions offer improved modelling near the distribution mode compared to standard exponential and gamma distributions. Fig. 7 illustrates the selected simulation distributions with 10000 points for each, along with fitted exponential and gamma distributions for visual comparison.

In the following simulation investigations, particular attention is given to smaller sample sizes, $n < 1000$, essential for sub-model analysis and for comparing fitting performance in cases where larger models could lead to overfitting the data.

### 7.1. Flexible body exponential

The summary statistics for the ML estimates are presented in Table 3 for the respective experiments. These estimates are obtained from 1000 samples drawn from the $X \sim FBE(10, 4)$ distribution. It is apparent that the $\alpha$ parameter estimate exhibits the largest bias and RMSE for all sample sizes. This bias and RMSE could be potentially problematic compared to the exponential distribution body shape of $\alpha = 1$ for $n < 250$. However, for larger sample sizes, $n \geq 250$, the mean of the fitted $\alpha$ estimates approaches 4, with RMSE values below or equal to 1, which can be considered significantly different to the exponential body shape of $\alpha = 1$. As the sample size increases typically both, the bias decreases in absolute value and the RMSE decreases.

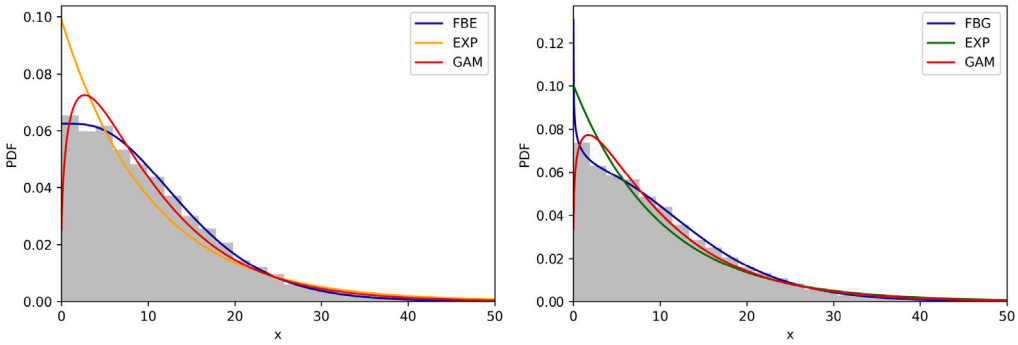


**Fig. 7.** Histogram of a sample of 10000 data points from the $X \sim FBE(10, 4)$ and $X \sim FBG(10, 4, 0.9)$ distributions, accompanied by their respective theoretical PDF as well as fitted exponential and gamma PDFs for a visual comparison.

**Table 3**
Summary statistics of fitted ML estimates for simulated FBE distribution samples.

| | Parameter | Mean | Median | RMSE | Bias | $n$ |
|---|---|---|---|---|---|---|
| $\sigma$ | 10 | 9.98158 | 9.98446 | 0.73030 | −0.02098 | 100 |
| $\alpha$ | 4 | 4.89531 | 4.29067 | **2.27048** | **0.76626** | 100 |
| $\sigma$ | 10 | 9.97820 | 9.94519 | 0.43892 | −0.02337 | 250 |
| $\alpha$ | 4 | 4.30607 | 4.09371 | **1.17272** | **0.26747** | 250 |
| $\sigma$ | 10 | 10.00728 | 10.01625 | 0.32881 | 0.00686 | 500 |
| $\alpha$ | 4 | 4.13984 | 4.03276 | **0.75055** | **0.12396** | 500 |
| $\sigma$ | 10 | 10.00448 | 10.00255 | 0.25424 | 0.00417 | 750 |
| $\alpha$ | 4 | 4.10181 | 4.04988 | **0.63314** | **0.09373** | 750 |

**Table 4**
Summary statistics of fitted ML estimates for simulated FBG distribution samples.

| | Parameter | Mean | Median | RMSE | Bias | $n$ |
|---|---|---|---|---|---|---|
| $\sigma$ | 10 | 9.96374 | 9.95726 | 0.78203 | −0.03626 | 100 |
| $\alpha$ | 4 | 4.96960 | 4.17904 | **3.49751** | **0.96960** | 100 |
| $\nu$ | 0.9 | 0.96335 | 0.91335 | 0.20629 | 0.06335 | 100 |
| $\sigma$ | 10 | 10.00214 | 9.99936 | 0.49268 | 0.00214 | 250 |
| $\alpha$ | 4 | 4.35579 | 4.08605 | **1.64725** | **0.35579** | 250 |
| $\nu$ | 0.9 | 0.91477 | 0.90614 | 0.09314 | 0.01477 | 250 |
| $\sigma$ | 10 | 9.99968 | 9.99205 | 0.34208 | −0.00032 | 500 |
| $\alpha$ | 4 | 4.24371 | 4.11546 | **1.07965** | **0.24371** | 500 |
| $\nu$ | 0.9 | 0.90437 | 0.90203 | 0.05930 | 0.00437 | 500 |
| $\sigma$ | 10 | 9.99986 | 10.00552 | 0.28968 | −0.00014 | 750 |
| $\alpha$ | 4 | 4.10922 | 4.02772 | **0.83267** | **0.10922** | 750 |
| $\nu$ | 0.9 | 0.90571 | 0.90272 | 0.04898 | 0.00571 | 750 |

### *7.2. Flexible body gamma*

The summary statistics for the ML estimates are presented in Table 4 for the respective experiments. These estimates are obtained from 1000 samples drawn from the $X \sim FBG(10, 4, 0.9)$ distribution. It is evident that the body shape parameter $\alpha$ shows a larger RMSE and bias compared to the scale parameter $\sigma$ and the left tail shape parameter $\nu$ for all sample sizes. The bias and RMSE could be potentially problematic compared to the gamma distribution body shape of $\alpha = 1$ for $n < 250$. For sample sizes of $n \geq 500$, the mean of the estimated $\alpha$ values is close to 4, with RMSE values below or close to 1, which may be considered significantly different to the gamma body shape of $\alpha = 1$. As expected, generally the bias decreases in absolute value and the RMSE decreases as the sample size increases.

## 8. FIG applications

In this section, the FIG is fitted to commonly available benchmark data to compare the flexibility with competing distributions. The competitor models are the log-normal (LN), gamma (GA), inverse Gaussian (IG; [40]) and generalised inverse Gaussian (GIG; [41]). These models are some of the most famous for modelling positive data; see [42] and the review paper [43]. For a detailed list of where the IG has been successfully implemented, see [36,44]. The evaluation of fit is done by computing both in-sample and

**Table 5**
Summary statistics for hand grip strength data.

| Min | Max | Median | Mean | Std | Pearson skewness | Pearson kurtosis | Count |
|---|---|---|---|---|---|---|---|
| 7 | 60 | 24 | 25.71 | 8.85 | 0.81 | 3.41 | 3766 |

**Table 6**
In- and out-of-sample metrics of distributions fitted to hand grip strength data.

| Distribution | $LL_{is}$ | $AIC_{is}$ | $BIC_{is}$ | $LL_{os}$ |
|---|---|---|---|---|
| LN | −11976.363 | 23 956.726 | 23 968.983 | −1346.750 |
| IG | −11974.224 | 23 952.447 | 23 964.704 | −1352.182 |
| GIG | −11973.171 | 23 952.342 | 23 970.728 | −1349.809 |
| GA | −11997.051 | 23 998.102 | 24 010.359 | −1342.912 |
| GG | −11982.560 | 23 971.120 | 23 989.506 | −1342.772 |
| FIG | −11976.559 | 23 961.118 | 23 985.633 | −1344.217 |

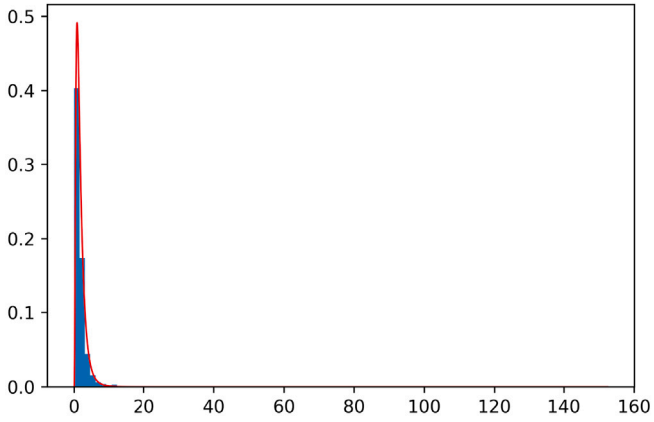


**Fig. 8.** Histogram and fitted FIG PDF to Danish building fire loss data.

out-of-sample validation metrics. The in-sample statistics are the Akaike information criterion ($AIC_{is}$) and Bayesian information criterion ($BIC_{is}$) computed on the subset of data used for estimation; see [45,46]. The out-of-sample LL ($LL_{os}$) is computed on a 10% subset of data excluded from estimation. This is done to ensure robust goodness of fit analysis and the prevention of overfit of the final models [47]. The numerical estimation starting parameters will be the ML estimates of the GG distribution since it is a sub-model of the FIG. The application is implemented using both R and Python, with the libraries **NumPy** [38], **Scipy** [39], and **mpmath** [48] being used in Python. The inherent high abstraction of R and Python, combined with the evaluation of Meijer's G function, causes the estimation of parameters to run in minutes instead of seconds.

*Hand grip strength*

The data consists of the hand grip strength of English school boys. The data is provided in the **gammlss.data package**, available online at https://cran.r-project.org/web/packages/gamlss.data, accessed 23 July 2022. The summary statistics of hand grip strength are given in Table 5. The in-sample criterion and out-of-sample $LL_{os}$ are tabulated in Table 6. In this application, the in-sample metrics are the lowest for the IG and GIG. However, the $LL_{os}$ favours the gamma, GG, and FIG because they are higher than the IG and GIG. It can therefore be concluded that the distributions perform similarly, with preference to be given to the simpler log-normal and gamma distributions due to parsimony. The fitting of the generalised models as competitors remains important since we would not know whether a more complex model is necessary if we do not fit one.

*Danish fire losses*

The data consists of the Copenhagen Reinsurance fire losses for the period from 1980 to 1990. The claim amount in millions of Danish Krone is divided into building, contents, and profit loss. The data is provided in the **CASdatasets** package, available at http://cas.uqam.ca/, accessed 25 July 2022. The summary statistics of the different loss types are given in Table 7. An illustration of the distributional shape shown by the histogram and fitted FIG PDF is shown in Fig. 8. It is worth noting that multiple views of the histogram were attempted, but the current plot provides the best illustration.

**Table 7**
Summary statistics for Danish fire losses data.

| Type | Min | Max | Median | Mean | Std | Pearson skewness | Pearson kurtosis | |
|---|---|---|---|---|---|---|---|---|
| Buildings | 0.02 | 152.41 | 1.33 | 2.01 | 4.72 | 22.98 | 660.40 | 1990 |
| Content | 0.01 | 132.01 | 0.58 | 1.71 | 5.43 | 15.50 | 321.96 | 1679 |
| Profit | 0.01 | 61.93 | 0.28 | 0.88 | 3.06 | 15.23 | 292.13 | 616 |

**Table 8**
In- and out-of-sample metrics of distributions fitted to Danish fire losses data.

| Type | Distribution | $LL_{is}$ | $AIC_{is}$ | $BIC_{is}$ | $LL_{os}$ |
|---|---|---|---|---|---|
| Buildings | LN | −2646.000 | 5296.000 | 5306.987 | −262.301 |
| | IG | −2849.905 | 5703.811 | 5714.797 | −278.373 |
| | GIG | −2848.965 | 5703.930 | 5720.410 | −277.869 |
| | GA | −2964.218 | 5932.437 | 5943.423 | −281.531 |
| | GG | −2675.870 | 5357.739 | 5374.219 | −263.656 |
| | FIG | −2649.058 | 5306.117 | 5328.090 | −260.759 |
| Content | LN | −1862.040 | 3728.080 | 3738.707 | −205.878 |
| | IG | −2100.065 | 4204.129 | 4214.757 | −213.877 |
| | GIG | −2032.208 | 4070.415 | 4086.357 | −220.340 |
| | GA | −2185.560 | 4375.121 | 4385.748 | −252.081 |
| | GG | −1895.756 | 3797.512 | 3813.453 | −212.069 |
| | FIG | −1879.272 | 3766.544 | 3787.799 | −209.191 |
| Profit | LN | −283.271 | 570.542 | 579.154 | −16.329 |
| | IG | −327.101 | 658.203 | 666.815 | −18.264 |
| | GIG | −312.282 | 630.564 | 643.483 | −18.597 |
| | GA | −395.842 | 795.683 | 804.296 | −32.108 |
| | GG | −292.055 | 590.110 | 603.029 | −17.962 |
| | FIG | −288.890 | 585.780 | 603.005 | −17.474 |

The in-sample criterion and out-of-sample $LL_{os}$ are tabulated in Table 8. In this application, the FIG is a clear favourite in all types of fire losses since the in- and out-sample metrics coincide. That is, the in-sample metrics are lowest for the FIG as well as the highest for the out-of-sample metric $LL_{os}$. It can therefore be concluded that for these loss data, a generalised model is more appropriate.

## 9. Conclusions

In this paper, we address the need for more flexible distributions without compromising on desirable distribution traits for positive data (Section 1). The exploration of Weibullisation, power weighting, and a stochastic representation that give rise to the FIG distribution is given (Section 2). The FIG has desirable properties such as a low number of interpretable parameters, simple tractability, and finite moments. We provide many common statistical properties for using the FIG in practice. These are the PDF, CDF, moments, MGF, and ML estimation equations (Sections 3 and 4). The roles of the tail parameters are investigated mathematically in Section 5. Regarding identifiability, a proof that the FIG parameters is an identifiable model is provided in Section 6. An evaluation of the ML estimation of FIG sub-models, including the FBE and FBG sub-models, is done via simulation (Section 7). The applicability of the FIG is demonstrated on hand grip strength and insurance loss data where the FIG provides a competitive fit in comparison to the IG and GIG distributions (Section 8). Points for further research may include finite mixture modelling, kernel density smoothing, outlier detection, gamma regression, and reliability modelling. Further, in the future, to make the code faster and more efficient, we plan on using compiled languages such as C or C++ instead of interpreted languages such as R or Python.

## Declaration of competing interest

The author assure that we have no financial, personal, or professional interests that could compromise the impartiality and integrity of the research process.

## Data availability

Data will be made available on request.

## Acknowledgements

We would like to thank Prof. Angelo Spina from the Scientific High School E. Boggio Lera, Catania, Italy, for his assistance in determining the identifiability of the FIG distribution.

*Financial disclosure*

The following funding sources are relevant: the National Research Fund no. SRUG190308422768; Statomet, University of Pretoria; Centre of Excellence in Mathematical and Statistical Sciences, University of the Witwatersrand; Centre for Environmental Studies, Department of Geography, Geoinformatics and Meteorology, University of Pretoria; Iran National Science Foundation no. 4015320.

## Appendix. Lemmas

**Lemma 1.** *Let $\alpha, \beta > 0$. Then the following limit holds true*

$$\lim_{x\to\infty} x^k \Gamma\left(\frac{\alpha}{\beta}, x^\beta\right) = 0 \quad \text{for } k \in \mathbb{R}. \tag{A.1}$$

*If $k \le 0$ both factors on the left-hand side of (A.1) tend to zero as $x$ tends to infinity. If $k > 0$, by L'Hôpital's rule*

$$\lim_{x\to\infty} x^k \Gamma\left(\frac{\alpha}{\beta}, x^\beta\right) = \lim_{x\to\infty} \frac{x^{\alpha+\beta+k-1}}{e^{x^\beta}} \cdot \frac{\beta}{k} = 0$$

**Lemma 2.** *Let $\alpha, \beta > 0$, then the following integral identity holds true*

$$\int_x^\infty t^r \Gamma\left(\frac{\alpha}{\beta}, t^\beta\right) dt = \frac{\Gamma\left(\frac{\alpha+r+1}{\beta}, x^\beta\right) - x^{r+1}\Gamma\left(\frac{\alpha}{\beta}, x^\beta\right)}{r+1}. \tag{A.2}$$

*Let $y = t^\beta$, which implies $t = y^{\frac{1}{\beta}}$. Integrating by parts, where $v'(y) = \frac{r+1}{\beta} y^{\frac{r+1}{\beta}-1}$ and $u(y) = \Gamma(\alpha/\beta, y)$. The latter implies that $v(y) = y^{\frac{r+1}{\beta}}$ and $u'(y) = -y^{\frac{\alpha}{\beta}-1}e^{-y}$. The integral is evaluated as*

$$\int_x^\infty t^r \Gamma\left(\alpha/\beta, t^\beta\right) dt = (r+1)^{-1}\, y^{\frac{r+1}{\beta}} \Gamma(\alpha/\beta, y)\Big|_{x^\beta}^\infty - (r+1)^{-1} \int_{x^\beta}^\infty y^{\frac{r+1}{\beta}} \cdot \left(-y^{\frac{\alpha}{\beta}-1}e^{-y}\right) dy.$$

*Noting from Lemma 1 that $\lim_{x\to\infty} y^{\frac{r+1}{\beta}} \Gamma(\alpha/\beta, y) = 0$ the result follows.*

**Lemma 3.** *Let $\alpha, \beta > 0$. Then the following integral identity holds true*

$$\int_0^\infty x^r \Gamma\left(\frac{\alpha}{\beta}, x^\beta\right) dx = \frac{\Gamma\left(\frac{\alpha+r+1}{\beta}\right)}{r+1}. \tag{A.3}$$

*The result follows by evaluating the limit, $\lim_{t\to 0^+}$, over the integral in Lemma 2.*

## References

[1] Stacy EW, Hoshkin N. A generalization of the Gamma distribution. Ann Math Stat 1962;33(3):1187–92.
[2] Amoroso L. Ricerche intorno alla curva dei redditi. Ann Mat Pura Appl 1925;2(1):123–59.
[3] Lee MT, Gross AJ. Lifetime distributions under unknown environment. J Stat Plan Inference 1991;29(1–2):137–43.
[4] Barkauskas D, Kronewitter S, Lebrilla C, Rocke D. Analysis of MALDI FT-ICR mass spectrometry data: A time series approach. Anal Chimica Acta 2009;648(2):207–14.
[5] Almpanidis G, Kotropoulos C. Phonemic segmentation using the generalised Gamma distribution and small sample Bayesian information criterion. Speech Commun 2008;50(1):38–55.
[6] Chen Y, Karagiannidis G, Lu H, Cao N. Novel approximations to the statistics of products of independent random variables and their applications in wireless communications. IEEE Trans Veh Technol 2011;61(2):443–54.
[7] Ali M, Woo J, Nadarajah S. Generalized gamma variables with drought application. J Korean Stat Soc 2008;37(1):37–45.
[8] Kleiber C, Kotz S. Statistical size distributions in economics and actuarial sciences. vol. 470, John Wiley & Sons; 2003.
[9] Kaneko R. Elaboration of the Coale-McNeil nuptiality model as the generalized log gamma distribution: A new identity and empirical enhancements. Demograph Res 2003;9:223–62.
[10] Ley C. Flexible modelling in statistics: past, present and future. J Soc Francaise Statistique 2015;156(1).
[11] Jones M. On families of distributions with shape parameters. Int Stat Rev 2015;83(2):175–92.
[12] McLeish DL. A robust alternative to the normal distribution. Canad J Stat 1982;89–102.
[13] Punzo A, Bagnato L. The multivariate tail-inflated normal distribution and its application in finance. J Stat Comput Simul 2021;91(1):1–36.
[14] Wagener M, Bekker A, Arashi M. Mastering the body and tail shape of a distribution. Mathematics 2021;9(21):2648.
[15] Ley C, Babić S, Craens D. Flexible models for complex data with applications. Annu Rev Stat Appl 2021;8:369–91.
[16] Malik HJ. Exact distribution of the quotient of independent generalized Gamma variables. Canad Math Bull 1967;10(3):463–5.
[17] Saieed H, Abdulla M, Hayawi H. Inverse generalized Gamma distribution with it's properties. Iraqi J Stat Sci 2020;17(31):64–71.
[18] Bilankulu V, Bekker A, Marques F. The ratio of independent generalized gamma random variables with applications. Comput Math Methods 2021;3(1):e1061.
[19] Consul PC, Jain GC. On the log-gamma distribution and its properties. Stat Hefte 1971;12(2):100–6.
[20] Prentice RL. A log gamma model and its maximum likelihood estimation. Biometrika 1974;61(3):539–44.
[21] Bell BM. Generalized gamma parameter estimation and moment evaluation. Comm Statist Theory Methods 1988;17(2):507–17.
[22] Agarwal S, Kalla S. A generalized gamma distribution and its application in reliability. Commun Stat-Theory Methods 1996;25(1):201–10.
[23] Pauw J, Bekker A, Roux J. Densities of composite Weibullized generalized gamma variables: theory and methods. South Afr Stat J 2010;44(1):17–42.

[24] Cordeiro GM, Ortega EM, Silva GO. The exponentiated generalized gamma distribution with application to lifetime data. J Stat Comput Simul 2011;81(7):827–42.
[25] De Pascoa MAR, Ortega EM, Cordeiro GM. The kumaraswamy generalized gamma distribution with application in survival analysis. Stat Methodol 2011;8(5):411–33.
[26] Cordeiro GM, Castellares F, Montenegro LC, de Castro M. The beta generalized gamma distribution. Statistics 2012;47(4):888–900.
[27] Cordeiro GM, Pescim R, Ortega E. The kummer beta generalized Gamma distribution. J Data Sci 2014;12(4):661–97.
[28] Lucena SE, Herm A, Cordeiro GM. The transmuted generalized gamma distribution: Properties and application. J Data Sci 2015;13(1):187–206.
[29] Priyadarshani HA, Oluyede BO. Theoretical properties of the weighted generalized gamma and related distributions. Probab Engrg Inform Sci 2015;29(3):421–32.
[30] Vallejos A, Ormazábal I, Borotto FA, Astudillo HF. A new $\kappa$-deformed parametric model for the size distribution of wealth. Phys A 2019;514:819–29.
[31] Kaniadakis G. New power-law tailed distributions emerging in $\kappa$-statistics. Europhys Lett 2021;133(1):10002.
[32] Barriga G, Cordeiro G, Dey D, Cancho V, Louzada F, Suzuki A. The marshall-olkin generalized gamma distribution. Commun Stat Appl Methods 2018;25(3):245–61.
[33] Bakery AA, Zakaria W, Mohamed OMKSK. A new double truncated generalized Gamma model with some applications. J Math Univ Tokushima 2021;2021:27.
[34] Pham-Gia T, Duong Q. The generalized beta- and F-distributions in statistical modelling. Math Comput Modelling 1989;12(12):1613–25.
[35] Subbotin MT. On the law of frequency of error. Mathematicheskii Sbornik 1923;31(2):296–301.
[36] Johnson N.L. N, Kotz S, Johnson NL. Continuous univariate distributions. AGRIS 1970.
[37] Gradshteyn I, Ryhzhik I. Table of integrals, series and products. Cambridge, MA, USA: Academic Press; 2007.
[38] Harris CR, Millman KJ, van der Walt SJ, Gommers R, Virtanen P, Cournapeau D, et al. Array programming with NumPy. Nature 2020;585:357–62.
[39] Virtanen P, Gommers R, Oliphant TE, Haberland M, Reddy T, Cournapeau D, et al., SciPy 10 Contributors SciPy 1.0: Fundamental algorithms for scientific computing in python. Nature Methods 2020;17:261–72.
[40] Samuelson PA, DM, EA. Louis Bachelier's theory of speculation: the origins of modern finance. 2006.
[41] Jorgensen B. Statistical properties of the generalized inverse Gaussian distribution. vol. 9, Springer Science & Business Media; 2012.
[42] Tweedie M. Statistical properties of inverse Gaussian distributions. I. Ann Math Stat 1957;28(2):362–77.
[43] Folks J, Chhikara R. The inverse Gaussian distribution and its statistical application—A review. J R Stat Soc Ser B Stat Methodol 1978;40(3):263–75.
[44] Seshadri V. The inverse Gaussian distribution: Statistical theory and applications. vol. 137, Springer Science & Business Media; 2012.
[45] Akaike H. A new look at the statistical model identification. IEEE Trans Autom Control 1974;19(6):716–23.
[46] Schwarz G. Estimating the dimension of a model. Ann Statist 1978;6(2):461–4.
[47] Rigby RA, Stasinopoulos DM. Generalized additive models for location, scale and shape, (with discussion). Appl Stat 2005;54:507–54.
[48] Johansson F. Mpmath: a python library for arbitrary-precision floating-point arithmetic (version 1.1.0). 2018.